

www.acsami.org Research Article

Co-Casting Highly Selective Dual-Layer Membranes with Disordered Block Polymer Selective Layers

Nicholas Hampu, Jay R. Werber, and Marc A. Hillmyer*



Cite This: ACS Appl. Mater. Interfaces 2020, 12, 45351–45362



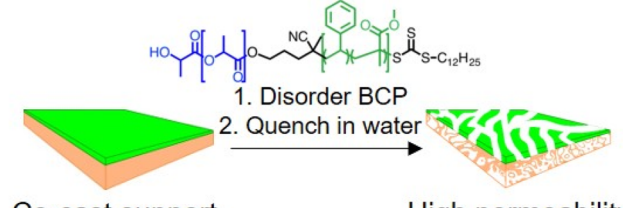
ACCESS

III Metrics & More



s Supporting Information

ABSTRACT: Highly selective and water permeable dual-layer ultrafiltration (UF) membranes comprising a disordered poly-(methyl methacrylate-stat-styrene)-block-poly(lactide) selective layer and a polysulfone (PSF) support layer were fabricated using a co-casting technique. A dilute solution of diblock polymer was spin coated onto a solvent-swollen PSF layer, rapidly heated to dry and disorder the block polymer layer, and subsequently immersed into an ice water coagulation bath to kinetically trap the disordered state in the block polymer selective layer and precipitate the support layer by nonsolvent-induced phase separation.



Co-cast support and selective layers High permeability High selectivity

Subsequent removal of the polylactide block generated porous membranes suitable for UF. The permeability of these dual-layer membranes was modulated by tuning the concentration of the PSF casting solution, while the size-selectivity was maintained because of the narrow pore size distribution of the self-assembled block polymer selective layer. Elimination of the thermal annealing step resulted in a dramatic increase in the water permeability without adversely impacting the size-selectivity, as the disordered nanostructure present in the concentrated casting solution was kinetically trapped upon rapid drying. The co-casting strategy outlined in this work may enable the scalable fabrication of block polymer membranes with both high permeability and high selectivity.

KEYWORDS: ultrafiltration, block polymer, composite membrane, permeability-selectivity, order—disorder transition, co-casting

■ INTRODUCTION

Each year, inadequate water sanitation is estimated to account for ~1 million deaths globally. Furthermore, reliable access to clean water sources is expected to be further stressed by the effects of industrialization, population growth, and climate change. To meet the growing demand for clean and safe drinking water, membrane technologies have emerged as an effective and energy-efficient platform for the treatment of wastewater. 1-4 In particular, ultrafiltration (UF) membranes containing continuous pores with sizes ranging from approximately 1 to 100 nm have received extensive interest for the removal of critical water-borne species such as bacteria, viruses, and dissolved macromolecules from drinking water and wastewater. 4-6 UF membranes operate by a size-exclusion mechanism, where particles larger than the membrane pores are excluded and smaller species are able to permeate. Two principal metrics are typically used to assess UF membrane performance: permeability and selectivity. The ideal UF membrane would exhibit both high water permeability (defined as the water flux normalized to applied pressure difference) and high size-selectivity (defined as quantitative rejection of all particles larger than the average pore size). 1,2,4,7

Commercial UF membranes are typically prepared via nonsolvent-induced phase separation (NIPS), where a homopolymer solution is cast into a film and then immersed into a nonsolvent coagulation bath to induce phase separation and pore formation.^{3,8} These membranes demonstrate excellent water permeability because of their plurality of continuous pores. However, the stochastic nature of NIPS results in a broad pore size distribution, limiting the size-selectivity.^{1,7–9} To improve upon the selectivity of NIPS membranes, block polymers have emerged as an intriguing alternative because of their ability to self-assemble into regularly ordered domains of uniform size.^{5,10–12}

The implementation of block polymers into membrane technologies has been hindered by the scalability of existing fabrication and processing methods. Block polymer selective layers can be supported on pre-formed porous NIPS membranes by either direct solution casting (spin or blade coating) or by floating off thin films from a sacrificial substrate and placing them atop a support layer. 5,10,11,13,14 While successful on the lab-scale, practical challenges associated with solution-casting thin films onto porous supports or with

Received: July 30, 2020 Accepted: September 15, 2020 Published: September 28, 2020





floating off large, module-size films have proven to be limiting for scale-up. Additionally, continuous pores (i.e., pores that percolate from one side of the membrane to the other) are necessary to achieve high water permeability. However, typical ordered block polymer morphologies are either anisotropic cylinders that require post-processing alignment techniques to orient domains perpendicular to the substrate surface^{5,10,15} or are isotropic and bicontinuous (e.g., gyroid), yet require precise syntheses to reliably access. 16 Selectively swelling unaligned cylinder-forming block polymers has been shown to produce continuous pores without orienting the domains, but these systems still require coating onto porous substrates. 11,17-19 Alternatively, recent work has addressed these processing limitations by forming free-standing membranes of block polymers using evaporation-induced self-assembly followed by NIPS (SNIPS). These SNIPS membranes exhibit an integral and asymmetric structure comprising a thin selective layer with a narrow pore size distribution supported by a highly porous block polymer substructure. 12,20,21 While promising, SNIPS membranes can require large quantities of block polymer as well as stringent formulations, resulting in high material expenses. Additionally, it is relatively difficult to access small pore sizes (≤~10 nm) using SNIPS.²¹

Recently our group has reported that the fluctuating disordered state in block polymers can be kinetically trapped by either cross-linking above the order—disorder transition (ODT) temperature $(T_{\rm ODT})$ or by rapidly cooling from above the $T_{\rm ODT}$ to below the glass transition temperature $(T_{\rm g})^{.22-25}$ Upon the selective removal of one domain, a bicontinuous network of pores within a supporting glassy matrix was obtained. The resulting pores were shown to have a narrow size distribution, while their disordered and bicontinuous nature eliminated the need for domain alignment during UF membrane fabrication. ²²

Inspired by hybrid approaches for co-casting dual-layer membranes comprising a SNIPS-derived block polymer selective layer and a NIPS-derived homopolymer support layer (SNIPS/NIPS), 21,26,27 we now report the development of a membrane fabrication process that combines homopolymer NIPS and disordered block polymer self-assembly to produce membranes with both high water permeability and high sizeselectivity. We first casted a concentrated solution of a polysulfone (PSF) homopolymer to form a nascent support layer. While the PSF layer remained swollen in the solvent, a second layer of a poly(methyl methacrylate-stat-styrene)-blockpolylactide (SML) block polymer was spin coated from a dilute solution onto the PSF layer to form a dual-layer liquid film. The block polymer was then disordered, and the duallayer film was immersed in ice water to simultaneously (i) kinetically trap the disordered state in the block polymer selective layer and (ii) generate pores in the PSF support layer by NIPS. Subsequent removal of the polylactide (PLA) domain resulted in the formation of a porous selective layer that imparted high size-selectivity atop a porous NIPS support layer that provided mechanical strength and high water permeability. The overall coating process resembles processes currently used to fabricate commercial membranes with an additional step of coating the block polymer, offering a route to potentially improve the size-selectivity of UF membranes without requiring major changes to the membrane casting infrastructure. This proof-of-concept study could result in the scalable production of high-performing membranes, pending

translation to industrially relevant coating processes, such as machine, draw, and curtain coatings and hollow fiber spinning.

EXPERIMENTAL SECTION

Materials. Unless specifically noted, all chemicals were purchased from Sigma-Aldrich. 1,8-Diazabicycloundec-7-ene (DBU) was used without further purification. Azobisisobutyronitrile (AIBN) (98%) was recrystallized from methanol and dried under reduced pressure overnight. 4-Cyano-4-[(dodecylsulfanylthiocarbonyl)sulfanyl]pentanol was dried under reduced pressure overnight prior to use. Styrene (S) (≥99%, stabilized) and methyl methacrylate (MMA) (99%, stabilized) were passed through a basic alumina column prior to use. ±-Lactide (99%) was kindly provided by ALTASORB. ±-Lactide was recrystallized from toluene and stored under a N₂ atmosphere. All bulk solvents were purchased from Fisher Scientific and used as received, unless otherwise specified. Dichloromethane (DCM) was purified using a solvent system comprised of columns of activated alumina and molecular sieves. PSF, Udel P1700, was obtained from Solvay. Hollytex 3265, a nonwoven polyester, was used as a support for the PSF membrane and was kindly provided by Ahlstrom-Munksjö. Blue dextran standards were obtained from TdB Consultancy.

Instrumentation. Proton nuclear magnetic resonance (¹H NMR) spectroscopy experiments were performed on a Bruker AVANCE III HD nanobay AX-400 spectrometer equipped with a 5 mm BBO SmartProbe and a SampleXpress autosampler. Spectra of the polymers were acquired in CDCl₃ using tetramethylsilane as the reference. Sizeexclusion chromatography (SEC) analysis was performed in tetrahydrofuran (THF) at 25 °C using an Agilent 1260 Infinity liquid chromatograph system equipped with three Waters Styragel columns in series, as well as a Wyatt DAWN Heleos II 18-angle laser light scattering detector S4 and a Wyatt OPTILAB T-rEX refractive index detector. Small-angle X-ray scattering (SAXS) profiles were collected at the Advanced Photon Source (APS) at Argonne National Laboratories using the Sector 5-ID-D beamline, which is maintained by the DuPont-Northwestern-Dow Collaborative Access Team. The rheological response of the block polymers was evaluated on a Rheometrics ARES mechanical spectrometer equipped with an 8 mm parallel plate geometry. The oven was maintained under a nitrogen atmosphere to prevent thermal degradation of the sample. Scanning electron microscopy (SEM) micrographs were obtained on a Hitachi SU8230 cold FEG-SEM microscope with an accelerating voltage of 3 kV, an upper secondary electron detector, and a lateral resolution of 1.1 nm at a working distance of 5 mm. Before imaging, the samples were coated with 2-5 nm of Ir via sputtering using an ACE600 coater.

PLA-19 Synthesis. DCM (50 mL) and \pm -lactide (7.0 g, 118 molar equiv) were mixed in a 100 mL pressure vessel in a N₂-filled g l o v e b o x . I n a s e p a r a t e v i a l , 4 - c y a n o - 4 - [(dodecylsulfanylthiocarbonyl)sulfanyl]pentanol (0.16 g, 1 molar equiv) was dissolved in DCM (5 mL). After the \pm -lactide was completely dissolved, the chain transfer agent (CTA) solution was added to the pressure vessel, and the mixture was stirred for several minutes. The catalyst DBU (0.06 mL, 1 molar equiv) was then added to the solution, the pressure vessel was hermetically sealed, and the reaction was removed from the glovebox. The reaction mixture was stirred for 20 min at room temperature. The polymerization was then exposed to air, and benzoic acid (0.13 g, 2.5 molar equiv) was added to quench the reaction. The mixture was precipitated into excess methanol, filtered, and dried overnight at room temperature under reduced pressure.

SML-48 Synthesis. PLA-19 (0.3 g, 1 equiv) was dissolved in styrene (S, 0.13 g, 80 equiv) and MMA (0.40 g, 254 equiv) monomers in a 2 dram vial equipped with a septum. Following complete dissolution, the free radical initiator AIBN (0.65 mg, 0.25 equiv, 33 μ L as a 2 wt % solution in toluene) was added to the reaction mixture. The vial was then sealed and sparged with N₂ for 20 min before immersing it into a preheated silicone oil bath set to 80 °C. The polymerization was run for 5 h (approximately 40%

conversion of MMA), and the reaction was terminated by exposure to air. The polymer was diluted in THF, precipitated into methanol, and dried overnight under reduced pressure at $100\,^{\circ}\text{C}$.

SAXS Measurements. Scattering experiments were performed using X-rays of wavelength 0.76 Å, and the scattering intensity was collected on a 2D Mar CCD detector. Sample-to-detector distances were calibrated using a silver behenate standard. Intensity as a function of the wave vector, q, where $q=(4\pi/\lambda)\sin(\theta/2)$ (θ is the scattering angle and λ is the X-ray wavelength), was obtained by azimuthally integrating the 2D patterns. For the quenched samples, SAXS profiles were collected at room temperature by directly using a monolith of the materials. For the measurement of the $T_{\rm ODT}$, the sample was loaded into a quartz capillary and annealed overnight under reduced pressure at 100 °C. The capillary was mounted in a Linkam heating stage for variable temperature measurements. The sample was equilibrated for at least 2 min at each temperature prior to data collection.

Gas Sorption Measurements. The nitrogen adsorption isotherm was obtained on a Quantachrome Autosorb iQ (Boynton Beach, FL) instrument at the temperature of liquid nitrogen (77.3 K). The sample was loaded in 6 mm stems and degassed for 20 h at room temperature before measurement using a turbomolecular pump. The Brunauer–Emmett–Teller (BET) specific surface area was obtained from the adsorption branch from $P/P_0=0.05-0.35$. The mesopore size distribution was estimated using a quenched solid density functional theory (QSDFT) kernel for the adsorption branch of nitrogen on carbon using a cylindrical pore model.

Membrane Preparation. An approximately 6 cm by 6 cm square of a nonwoven polyester support was cut from a larger sheet using scissors. This piece was then mounted on top of a 7.5 cm by 7.5 cm square glass plate and secured using an electrical tape. Care was taken to ensure that the polyester support remained flat against the glass plate to prevent bubble and hole formation during membrane casting. The glass plate was then placed on top of a spin coater and secured by pulling vacuum. The polyester film was prewet with a small amount (approximately 0.1 mL) of dimethyl formamide (DMF) to promote spreading of the PSF solution across the support and to prevent defect formation.⁶ The PSF support layer solution (approximately 1 mL) was dropped onto the center of the static polyester film. The film was accelerated at a rate of 500 rpm s⁻¹ and spin coated at 500 rpm for 5 s using a Brewer Science Cee 200 spin coater. Immediately following the completion of the process, the block polymer selective layer solution was filtered through a 0.22 μ m syringe and dropped in the center of the DMF-swollen PSF layer in a static dispense. Again, the film was accelerated at a rate of 500 rpm s⁻¹ and spin-coated at 500 rpm for 5 s. Following both coating steps, a liquid was observed on the walls of the spin coater, suggesting that the solvent was lost by viscous flow (i.e. "spin off").

Following the completion of both spin-coating steps, two liquid layers should be present: a denser and more viscous PSF layer swollen in DMF on the bottom and a less viscous P(MMA-s-S)-b-PLA layer swollen in THF on the top. Two different thermal processing methods were then examined to generate the final membrane. In the thermally annealed system, the film was moved to a covered and preheated hot plate set to 150 °C for 10 s to ensure complete THF removal and then immersed in an ice water coagulation bath to both precipitate the PSF support layer and vitrify the P(MMA-s-S)-b-PLA selective layer. In the as-cast system, the film sat for 10 s at room temperature before immersion in the ice water coagulation bath.

Following precipitation, all membranes remained in the water bath for at least 1 h prior to further experiments. For water flux and dextran rejection experiments, a 2.5 cm diameter disc was cut from the center of the larger sheet. The membranes were then immersed in a 2 M NaOH solution in methanol/water (60/40~v/v) for 1 h to remove the PLA domains in the selective layer, generating pores.

Control membranes were made using an identical process, except that a PLA homopolymer was used instead of the P(MMA-s-S)-b-PLA block polymer for the second layer. Selective removal of PLA then resulted in a bare PSF support.

Water Flux Measurements. A 2.5 cm diameter disc of the etched UF membrane was loaded into an Amicon 8010 stirred cell. The cell was pressurized using N_2 gas to induce water flow through the membrane. The permeate was collected in a glass vessel placed on top of a mass balance that was interfaced to a computer. Water flux was measured based on the change in the mass of permeated water over the experimental time scale. Three different pressure differences were applied to the cell (0.25, 0.5, and 1 bar) to determine the relationship between applied pressure and water flux. Water permeability was calculated based on the slope of a linear fit to the water flux versus applied pressure data.

Dextran Rejection Experiments. Size rejection experiments were performed using fluorescently labelled dextran standards (blue dextran) of varying molar masses (4, 10, 40, 70, 110, and 400 kg mol⁻¹). Each blue dextran standard was dissolved in deionized water to a concentration of 0.5 mg cm⁻³ to form separate solutions. The solution was then added to the dry Amicon 8010 stirred cell containing the dual-layer membrane, stirred at 500 rpm, and pressurized to 0.5 bar. The permeate was collected in a clean glass vial. Rejection was determined using UV—vis spectroscopy based on the ratio of the absorbance of the permeate solution to the absorbance of the feed solution at the wavelength corresponding to maximum absorbance. This experimental protocol was repeated for every dextran molar mass to generate a rejection curve.

RESULTS AND DISCUSSION

Characterization of Porous Materials in Bulk. The SML block polymer used as the selective layer was synthesized by a reversible addition-fragmentation chain-transfer copolymerization of MMA and S from a PLA macro chain transfer agent following a previously reported procedure. 25 The diblock terpolymer architecture of SML-48 is appealing for the cocasting strategy outlined in this work as the segregation strength (χN) can be precisely tuned by adjusting the composition of the P(MMA-s-S) block. As a result, the disordered state can be readily accessed at temperatures appropriate for convenient membrane casting while still allowing the average pore size to be tailored for the intended application. Here, we focus on a single diblock polymer as a representative case with a number-average molar mass of the PLA block $(M_{n,PLA})$ of 19 kg mol⁻¹, a number-average molar mass of the P(MMA-s-S) block $(M_{n,P(MMA-s-S)})$ of 29 kg mol⁻¹, and a molar fraction of styrene in the P(MMA-s-S) block (XS) of 0.29, as determined by SEC and ¹H NMR end group analysis (Figures S1-S3). This diblock will be referred to as SML-48. Dynamic mechanical analysis (DMA) (Figure S4) and variable temperature SAXS (Figure S5) for SML-48 demonstrated clear evidence of microphase segregation, yet the absence of higher order SAXS peaks indicated a lack of longrange order. A small shoulder in the storage modulus (G') was observed around 130 °C by DMA, possibly signifying an ODT. However, the decrease in G' was noticeably less sharp than that typically observed at T_{ODT} , making the assignment of this feature as the ODT ambiguous.

To demonstrate that porous materials could be produced from this diblock, a monolithic sample of SML-48 was annealed in the disordered state at 150 $^{\circ}$ C and rapidly quenched in liquid nitrogen to kinetically trap disordered state composition fluctuations. Following quenching, the PLA domains were selectively removed by immersing the monolith in a 2 M solution of NaOH in H₂O/MeOH (40/60 v/v) overnight at room temperature. Room-temperature SAXS of the etched monolith displayed an increase in the scattered intensity as compared to the unetched precursor, while the scattering vector of the principal scattering peak, q^* , remained

unchanged (Figure 1). Additionally, a reticulated disordered morphology similar to other disordered and co-continuous

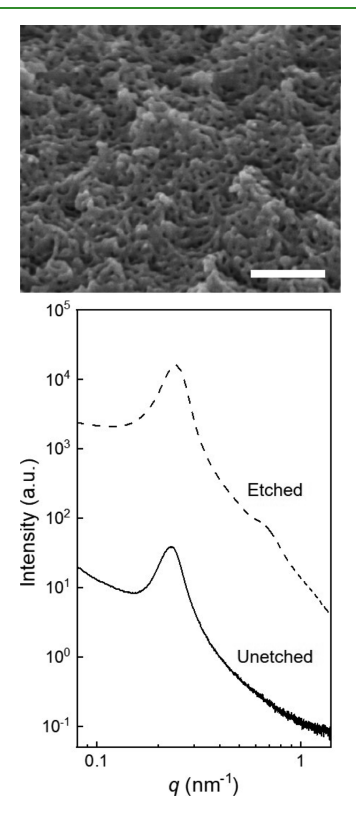


Figure 1. SEM of an etched monolith of SML-48 that was quenched from 150 $^{\circ}$ C (top). The scale bar corresponds to 200 nm, and the sample was coated with \sim 2 nm of Ir prior to imaging. Room-temperature SAXS patterns of monolithic samples of SML-48 that were quenched from 150 $^{\circ}$ C (bottom). Patterns were obtained both before (solid curve) and after (dashed curve) PLA etching.

polymers was observed by SEM after etching (Figure 1). These results indicated that a porous material templated by the block polymer structure was obtained.^{22,28} The three-dimensional continuity of these pores was confirmed by N₂ sorption analysis, which revealed a BET surface area of 83 m² g⁻¹ and a monomodal pore size distribution with a mode of 14 nm by QSDFT²⁹ (Figures S6 and S7) that was reasonably consistent with the pore size of 13 nm estimated by SEM. These results demonstrated that continuous pores with a narrow size distribution could be obtained from bulk samples, confirming the potential utility of SML-48 for membrane applications.

Preparation and Characterization of Thermally Annealed Dual-Layer Membranes. PSF was identified as an ideal homopolymer for the support layer. The high thermal and hydrolytic stabilities of PSF were compatible with the necessary thermal annealing, solvents, and etching conditions used for the SML-48 selective layer. In contrast, other polymers commonly used in NIPS membranes (e.g., polyacrylonitrile) were observed to undergo hydrolysis and a subsequent loss of dimensional stability upon exposure to the alkaline PLA-etching solution. DMF was selected as the solvent for the PSF layer as mechanically robust films could be obtained across a wide range of solution concentrations in contrast to other common PSF solvents, such as N-methyl pyrrolidone. Dual-layer membrane fabrication began with spin coating a concentrated PSF solution in DMF without any additional porogens onto a 6 cm by 6 cm nonwoven polyester backing that was prewet with DMF and taped to a 7.5 cm by 7.5 cm glass plate to ensure uniform spreading of the casting solution.³⁰ Spin coating was chosen as the coating procedure because of its ease and reproducibility at the lab scale. Liquid discharge was observed along the walls of the spin coater, indicating that film spreading occurred by viscous flow (i.e., "spin off") despite the relatively high solution viscosity and the slow spin speed. Next, a dilute solution of SML-48 in THF was filtered and deposited dropwise onto the static PSF/DMF layer before spin coating. The dual-layer liquid film was then annealed for a predetermined time (ca., 10 s) at 150 °C to disorder the SML-48 layer and evaporate residual THF (normal boiling point of 66 °C), while the PSF layer remained swollen in the much less volatile DMF (normal boiling point of 150 °C). After annealing, the film was immersed in ice water to trap the disordered state in the SML selective layer and precipitate the PSF layer by NIPS. An illustration of the process is provided in Figure 2.

To identify the effect that the support layer microstructure had on the dual-layer membrane permeability and selectivity, the concentration of the PSF solution was varied, while the coating parameters and annealing conditions for the selective layer were fixed. The concentration of the SML-48 solution was maintained at 0.1 wt % in THF. The annealing temperature and time for all membranes was 150 °C and 10 s, as higher temperatures and longer annealing times led to the formation of defective or dense membranes, likely due to excessive DMF evaporation. A spin coating rate of 500 rpm for 5 s with a ramp rate of 500 rpm s⁻¹ was selected for casting both layers as much faster rates or much longer times resulted in an undesirably high degree of PSF solution "spin off" from the support layer, leading to the formation of thin films with

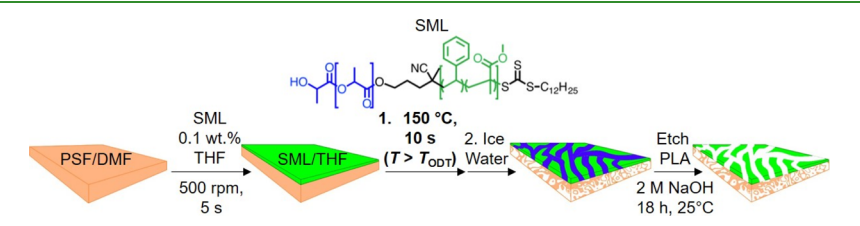


Figure 2. Schematic illustrating the thermally annealed fabrication procedure for the dual-layer membranes. First, a concentrated solution of PSF in DMF (typically 18-22 wt % PSF) is spin coated onto a nonwoven polyester backing at 500 rpm for 5 s. While the PSF layer is still swollen in DMF, a second layer of SML (chemical structure depicted) is spin coated from a 0.1 wt % solution in THF on top of the PSF/DMF layer at 500 rpm for 5 s. The dual-layer liquid film is annealed above $T_{\rm ODT}$ at $150~{\rm ^{\circ}C}$ for $10~{\rm s}$ before immersing in an ice water coagulation bath to precipitate the PSF layer and trap the bicontinuous, fluctuating disordered state in the SML selective layer. The PLA domains are then selectively removed using aqueous base to generate a porous selective layer.

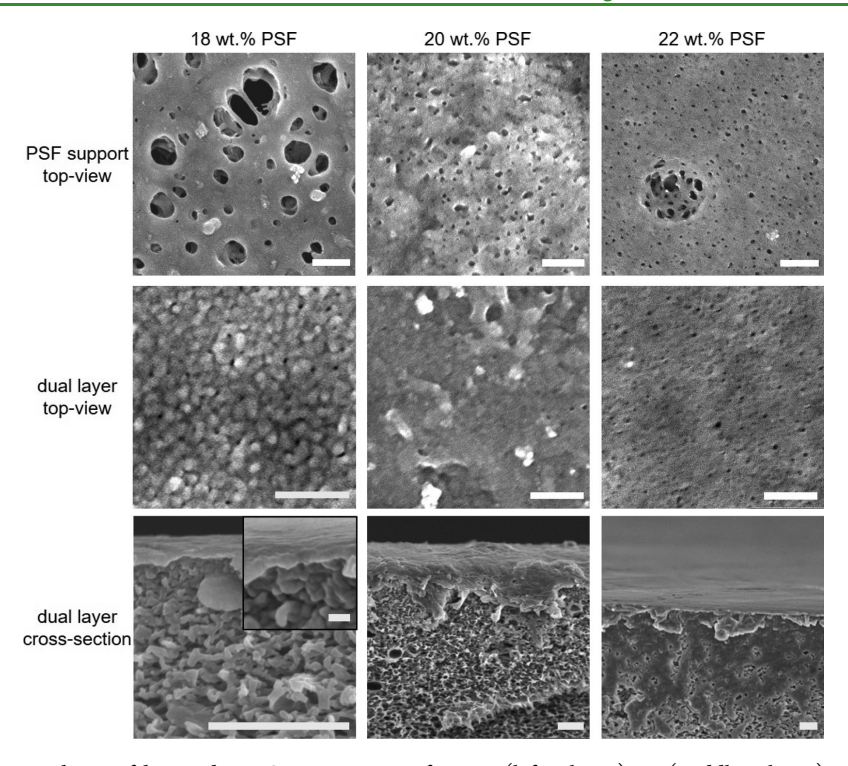


Figure 3. SEM of dual-layer membranes fabricated on PSF supports cast from 18 (left column), 20 (middle column), and 22 (right column) wt % solutions in DMF. Top-view images of the bare PSF support (fabricated by selectively removing the PLA-19 homopolymer surface layer as described) are presented in the top row, and top-view images of dual-layer membranes with block polymer selective layers are presented in the middle row. Cross-sectional images of cryo-fractured dual-layer membranes are presented in the bottom row. All membranes were selectively etched in 2 M NaOH to remove the PLA domains prior to imaging. The scale bars for the top-view images correspond to 200 nm, and the scale bars for the cross-sectional images correspond to 1 μ m. The inset shows the high-magnification cross-section of the PSF 18 wt % dual-layer membrane (the scale bar corresponds to 100 nm).

insufficient mechanical robustness for pressure-driven membrane operations. The concentration of the PSF solution was varied between 18 and 22 wt % in DMF. Lower concentrations of PSF (\leq 16 wt %) generally resulted in thin and highly defective membranes, while higher concentrations (\geq 25 wt %) resulted in dense and water impermeable membranes. Visually, the dual-layer membranes appeared white and macroscopically uniform following immersion in the ice water bath, generally resembling commercial membranes prepared by NIPS. Water was observed to form droplets rather than spontaneously spreading on the membrane surface, suggesting that the membrane had relatively low water wettability. Membranes were soaked in alcohol prior to flux and rejection measurements to promote pore wetting.

Following fabrication, the PLA domains in the selective layer were selectively removed to generate a porous structure. For comparative control samples, analogous bare PSF membranes were prepared using an identical procedure, except that the PLA homopolymer with a number-average molar mass of 19 kg mol⁻¹ (referred to as PLA-19) was used as the second layer instead of SML-48. These bare PSF membranes were subjected to the same thermal annealing process as dual-layer membranes with SML-48 selective layers. Subsequent etching of the PLA-19 homopolymer produced a PSF membrane that was expected to approximate the morphology of the underlying support layer in the dual membrane containing the block polymer. The surface morphologies of the porous membranes were then examined using SEM (Figure 3). The dual-layer membranes exhibited a noticeably different surface morphology than their corresponding support layers, consistent with a

selective layer being successfully deposited onto the PSF surface. The surface morphologies of the thin film dual-layer membranes were slightly different than those for the bulk SML-48 monolith, potentially reflecting the thinner and rougher nature of the thin films. Additionally, surface effects can be significant in thin films and could have affected the observed surface morphologies of the dual-layer membranes as compared to the bulk monolith shown in Figure 1a. The pore size of the PSF support layer significantly increased with decreasing PSF concentration, consistent with previously reported results.^{7,8,30} In contrast, the pore size of the block polymer selective layer was relatively unaffected by the concentration of the PSF casting solution.

Cross-sectional SEM images of cryo-fractured membranes confirmed the existence of a dual-layer film, comprising a thin and relatively dense SML selective layer on top of a thicker and more porous PSF support layer (Figure 3). Based on the membrane area and the volume of the block polymer solution deposited during spin-coating, a 300-nm-thick film (neglecting any polymer mass lost during "spin off") was expected. Deformation of the selective layer was observed in most crosssectional SEM images, making direct measurements of the selective layer thickness challenging. Samples with minimal selective layer deformation (e.g., 18 wt % PSF in Figure 3) allowed the film thickness to be estimated as approximately 100–200 nm (Figures 3, S8), which was reasonably consistent with the expected thickness. Slight variations in the film thickness were measured across the membrane area, suggesting that the selective layer thickness may be non-uniform. For

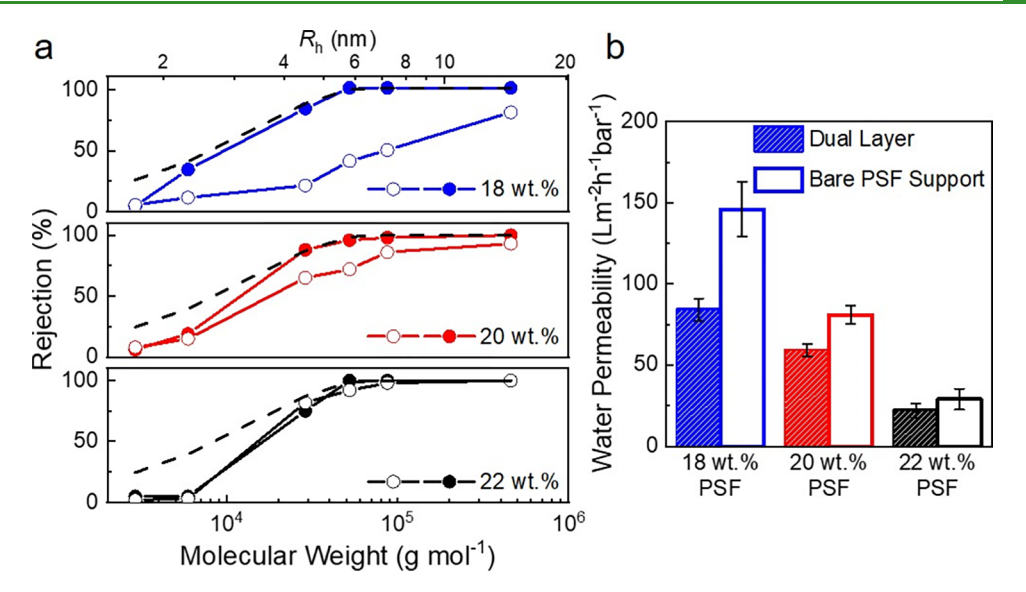


Figure 4. Rejection curves of fluorescently labeled dextran standards of dual-layer and PSF support membranes cast from 18 (blue), 20 (red), and 22 wt % (black) solutions of PSF in DMF (a). Closed circles correspond to dual-layer membranes with an SML-48 selective layer, and open circles correspond to bare PSF support membranes. The dashed black curve represents the theoretical rejection profile calculated using eq 1 for an isoporous membrane with a pore radius of 6.8 nm. Experimental rejection was determined based on the ratio of the maximum UV—vis absorbance for the permeate to the feed solution. The experimental data was then corrected using the mass transfer coefficient to account for concentration polarization, with the true rejection values shown in (a). Each data point was acquired for a feed solution comprising a single molar mass dextran standard. Water permeability of dual-layer (filled bars) and bare PSF support membranes (open bars) cast from 18 (blue), 20 (red), and 22 (black) wt % PSF (b). The permeability was determined based on the mean of three separate experiments, and the error bars correspond to the standard deviation.

samples exhibiting deformation, the cross-sectional SEM images demonstrate that two distinct layers are present.

Clear evidence of two layers in the cross-sectional SEM images along with the observed differences in surface morphology between the dual-layer and the bare PSF membranes suggested that the SML selective layer did not delaminate from the PSF support. In contrast, Nunes et al. reported that co-casting hybrid SNIPS/NIPS membranes resulted in poor adhesion and delamination of the block polymer selective layer when using industrially relevant support layers (e.g., polyacrylonitrile and polyethersulfone).²⁶ The dual-layer membranes examined in the present work comprise a solid block polymer film on top of a DMF-swollen PSF support prior to immersion in the water bath, resulting in a large contact area between the solvent swollen layers that presumably promotes adhesion. Additionally, the thermal annealing process and the miscibility of the DMF used to cast PSF with the THF used to cast SML-48 may promote a small amount of interdiffusion of the SML-48 selective layer into the PSF support layer at the interface. In comparison, the hybrid SNIPS/NIPS approach comprises highly porous surfaces on both sides of the [selective-layer]/[support-layer] interface, which minimizes the overall contact area and likely contributed to the previously reported poor adhesion.

Because of its uniformly sized pores, the self-assembled block polymer selective layer was expected to result in superior size-selectivity as compared to the bare PSF support fabricated using NIPS. To demonstrate this feature, each membrane was subjected to a series of feed solutions containing fluorescently labeled dextran standards of varying hydrodynamic radii. Rejection was determined based on the ratio of the maximum absorbance for the permeate solution to the feed solution using UV—vis spectroscopy. ^{23,24} The rejection profiles for the dual-layer membranes and their corresponding bare PSF supports

are presented in Figure 4a for membranes cast from 18, 20, and 22 wt % solutions of PSF in DMF. The experimentally measured rejection values were corrected using the mass transfer coefficient to account for concentration polarization to give true rejection values (see Supporting Information for further discussion).³¹ The high stirring speed (300 rpm) and the low applied pressure (0.5 bar) used during the filtration experiments minimized these concentration polarization effects. 10,31 For membranes cast from 18 to 20 wt % PSF in DMF, the rejection of high dextran molar masses (large hydrodynamic radii, R_h) was significantly higher for the duallayer membranes than for the bare supports. These results were consistent with the conclusion that the block polymer selective layer had a smaller average pore size that could more completely reject larger molecules.³² Furthermore, the rejection profile was significantly sharper for the dual-layer membranes because of the narrow pore size distribution of the self-assembled block polymer in comparison to the bare PSF support fabricated by NIPS. 7,9 The R_h that corresponds to the molecular weight cutoff (MWCO, defined as the molar mass where rejection is 90%) of the dual-layer membranes was \sim 5 nm, which was reasonably consistent with the mean pore radius of ~6.8 nm determined by QSDFT for bulk monoliths of SML-48 without the PSF support layer that were subjected to an identical annealing temperature (Figure S7). Indeed, the experimental data closely followed the theoretical prediction for the size-dependent rejection of solutes of radius, a, for an isoporous membrane with a uniform pore radius, r_p , of 6.8 nm¹10

$$R = 1 - \left[2 \left(1 - \frac{a}{r_{\rm p}} \right)^2 - \left(1 - \frac{a}{r_{\rm p}} \right)^4 \right] \exp \left[-0.7146 \left(\frac{a}{r_{\rm p}} \right)^2 \right]$$
(1)

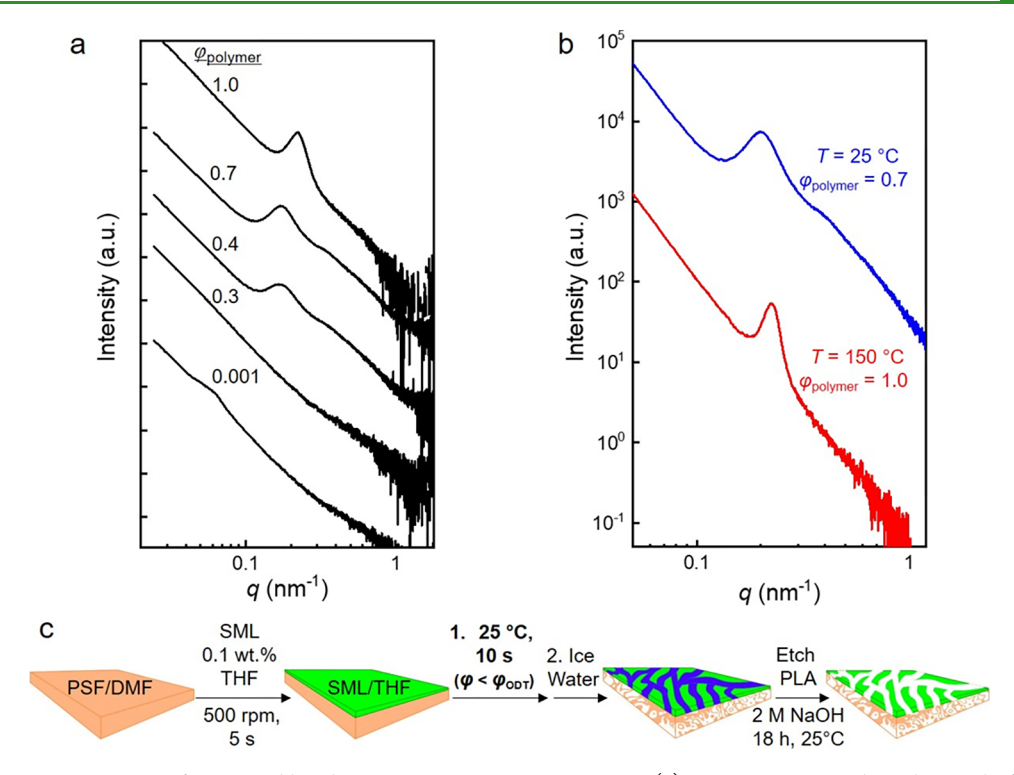


Figure 5. Room-temperature SAXS of SML-48 diluted in THF to various concentrations (a). φ_{polymer} corresponds to the weight fraction of SML-48 in the solution. Comparison between SAXS patterns obtained for SML-48 at 150 °C and $\varphi_{\text{polymer}} = 1.0$ (red curve) and at 25 °C and $\varphi_{\text{polymer}} = 0.7$ (blue curve) demonstrates that both the temperature and the solvent can be used to tune χN (b). Schematic illustrating the fabrication procedure for the as-cast dual-layer membranes (c). The process is identical to the one depicted in Figure 1, except that the solvent rather than the temperature is used to access the disordered state. After casting the SML-48 layer, the film rests for 10 s at 25 °C before immersing in an ice water coagulation bath. The PLA domains are then selectively removed using aqueous base to generate a porous selective layer.

Membranes cast from a 22 wt % solution of PSF in DMF exhibited only slight differences in dextran rejection between the dual-layer and bare PSF membranes (Figure 4a). A high rejection of dextran was observed in both cases. This high concentration of PSF likely resulted in a dense support layer with a comparable average pore size as SML-48, as evidenced by their similar MWCO. Overall, these results demonstrate that the uniform self-assembled block polymer domains significantly improve upon the size-selectivity of the bare support layer fabricated using a modified NIPS process.

One of the primary limitations of NIPS membranes is that they exhibit a significant trade-off between water permeability and size-selectivity because of their broad pore size distribution. 1,3,7 The presence of a small population of large pores in the active layer can enable the permeation of some solute particles that are larger than the average pore size. Therefore, the average pore size of a NIPS membrane needs to be significantly smaller than the hydrodynamic radius of the solute targeted for rejection to ensure complete removal. However, water permeability scales as r_p^4 for a fixed pore number density; even modest decreases in the average pore size result in large decreases in the permeability. 10,33 Consequently, NIPS membranes with smaller pore sizes enhance the solute rejection at the cost of significantly decreased water permeability. In contrast, the uniform pores of a block polymer selective layer should attenuate this tradeoff as a larger average pore size for an isoporous membrane can achieve an identical solute rejection as a NIPS membrane with much smaller pores. For the dual-layer membranes examined in this work, a sufficiently thin block polymer selective layer

imparts high size-selectivity without imposing a significant barrier to water transport.

Conversely, the water permeability of the dual-layer membrane is primarily dictated by the NIPS support without significantly altering the size-selectivity. In particular, we observed that the water permeability of the dual-layer membranes decreased from 84 ± 7 to 59 ± 4 to 22 ± 5 L m⁻² h⁻¹ bar⁻¹ as the concentration of the PSF casting solution increased from 18 to 20 to 22 wt % in DMF (Figures 4b and S8). A noticeably lower water permeability was observed prior to PLA removal and was attributed to water diffusion through PLA, 14 suggesting that the selective layer pores primarily resulted from removal of the self-assembled PLA domains rather than by NIPS. Analogous measurements for the bare PSF supports displayed a qualitatively similar trend, decreasing from 146 ± 17 to 81 ± 6 to 29 ± 7 L m⁻² h⁻¹ bar⁻¹ as the concentration of the PSF casting solution was increased from 18 to 20 to 22 wt % in DMF (Figures 4b and S9). Furthermore, SEM images of the bare PSF membranes displayed larger surface pores (Figure 3) and more porous substructures (Figure S11) for lower concentrations of PSF. These results suggest that the water permeability of the duallayer membranes is dependent upon the microstructure and the permeability of the PSF support. The presence of a highly concentrated (and potentially solvent-free) block polymer film may affect the diffusion of nonsolvent into the support layer during NIPS, altering the precipitation pathway. This may result in selective layer pores that are not completely aligned with those in the support layer, unlike in conventional NIPS. However, since the disordered morphology of the selective layer is isotropic and co-continuous, misaligned pores are expected to increase the effective path length (tortuosity) for water transport rather than completely block the porous channels.

Despite the strong dependence of the water permeability on the PSF concentration, the size-selectivity and MWCO of the dual-layer membranes remained essentially constant because of the nearly uniform pore size in the self-assembled SML-48 selective layer (Figure 4). In contrast, variations in the casting solution concentration for the bare PSF membranes resulted in a noticeable trade-off between the water permeability and the size-selectivity (Figures 4 and S9). These results confirmed that the rejection profile of the dual-layer membranes was dictated by the uniform pores in the selective layer, while the water permeability was primarily governed by the support layer. This introduces the possibility of significantly increasing the water permeability without compromising the selectivity, helping to minimize the large permeability-selectivity trade-off inherent to NIPS membranes. 10,12,14 We expect that the rejection profile and separation performance of the block polymer selective layer can be tuned while maintaining similar processing conditions by adjusting both the composition of the P(MMA-s-S) block and the overall block polymer molar mass. Previous work has reported average pore sizes ranging from approximately 10-20 nm for SML block polymers with similar T_{ODT} 's, where smaller pores are accessed by increasing the molar fraction of styrene and decreasing the overall molar mass.²⁵

Preparation and Characterization of As-cast Dual-**Layer Membranes.** The preceding sections have primarily utilized temperature as the stimulus for accessing the disordered state in the block polymer selective layer, where the selection of quench temperatures above T_{ODT} resulted in segregation strengths, χN , that were lower than the critical value of approximately 10.5. However, χN can be significantly reduced under isothermal conditions by swelling a block polymer in a neutral solvent. This screens the unfavorable enthalpic interactions between the two blocks at the domain interface and effectively lowers the T_{ODT} . We demonstrated this for bulk samples by hermetically sealing homogeneous mixtures of SML-48 and THF in hermetically sealed aluminum sample pans and then analyzing the mixtures using SAXS to monitor the development of the structure factor, S(q), as a function of the polymer concentration.³⁵ For very low concentrations (polymer weight fraction, $\phi_{
m polymer}$ < 0.4), featureless scattering patterns were observed, indicative of an unstructured system at these low effective values of χN (Figure 5a). As the concentration increased ($\phi_{
m polymer} \geq 0.4$), a broad peak in the SAXS patterns was observed that became increasingly sharp with increasing concentration, characteristic of more strongly segregated domains (Figure 5a). These results are consistent with an increase in χN with increasing polymer concentration, and they suggest that the solvent can serve a similar function as temperature in modulating the segregation strength of SML-48. Indeed, reasonably similar scattering patterns were observed for SML-48 heated to a temperature above $T_{
m ODT}$ in the melt state (T = 150 °C and $\phi_{
m polymer}$ = 1.0) and for SML-48 diluted below the $\phi_{
m ODT}$ in the solution state (T = 25 °C and $\phi_{\text{polymer}} = 0.7$) (Figure 5b).

Therefore, we anticipate that a disordered and bicontinuous morphology would be kinetically trapped in the selective layer at ambient temperature by rapidly drying a block polymer solution into a solid film during the spin coating process. ^{35–39} As the volatile THF solvent evaporates, the segregation

strength of the block polymer selective layer will increase due to the increasing volume fraction of the polymer. Eventually, at high block polymer concentrations, the system will solidify into a film, effectively vitrifying the morphology. If the drying process is sufficiently fast relative to the dynamics of the polymer chains, then the block polymer will be unable to order into its thermodynamically favored morphology prior to vitrification. Instead, it will be kinetically trapped in a disordered state that is expected to resemble the morphology that was observed after rapidly quenching from $T > T_{ODT}$. Indeed, disordered and worm-like morphologies have previously been observed in experiments and in simulations for block polymer thin films prepared after rapidly drying a dilute solution.³⁵⁻³⁹ THF is particularly well suited for this strategy as its low boiling point (66 °C) is expected to facilitate the rapid drying necessary to kinetically trap the disordered state by vitrification.

To demonstrate this experimentally, we modified the membrane fabrication procedure described in Figure 1 by eliminating the thermal annealing step. Instead, the dual-layer liquid film was equilibrated for approximately 10 s at room temperature following block polymer casting before it was immersed into an ice water coagulation bath and then selectively etched (Figure 5c). These solvent-disordered membranes will be referred to as "as-cast" membranes, while the previously discussed thermally annealed membranes prepared using the process outlined in Figure 1 will now be referred to as "annealed" membranes. Again, bare PSF membranes were fabricated using a procedure similar to the "as-cast" dual-layer membranes to facilitate comparisons.

The as-cast membranes were prepared using a 0.1 wt % solution of SML-48 in THF as the selective-layer casting solution and an 18 wt % solution of PSF in DMF as the support-layer casting solution as these concentrations resulted in the highest water permeability for the annealed membranes. Top-view SEM images of the annealed and as-cast membranes (Figure 6a) revealed similar surface morphologies for the block polymer selective layers regardless of their processing history, while cross-sectional SEM images showed a dual-layer morphology (Figure S12). These results suggested that the disordered morphology trapped in the as-cast membranes generally resembled the fluctuating disordered morphology obtained in the annealed membranes, supporting the conclusion that the solvent can be used as an alternative to temperature for tuning the segregation strength.³⁷

Effectiveness of the solvent approach was confirmed by the sharp rejection curves with nearly identical MWCO observed for both as-cast and annealed membranes, indicating that the block polymer selective layers had nearly uniform pores of similar size regardless of the thermal processing history (Figure 6). Despite their nearly identical rejection profiles, the water permeability of the as-cast membrane, $153 \pm 8 \text{ L m}^{-2} \text{ h}^{-1}$ bar⁻¹, was nearly twice that of the annealed membrane, $84 \pm 7 \text{ L m}^{-2} \text{ h}^{-1} \text{ bar}^{-1}$ (Figure 6b). Similar trends were observed for as-cast and annealed membranes with support layers cast from 20 to 22 wt % PSF solutions in DMF (Figures S13 and S14).

The significantly increased permeability of the as-cast membrane suggested that the thermal annealing process affected the phase behavior of the PSF layer, altering its precipitation pathway during NIPS and ultimately resulting in a less porous and less permeable substructure without significantly increasing the pore continuity of the block polymer selective layer. This was supported by a lower

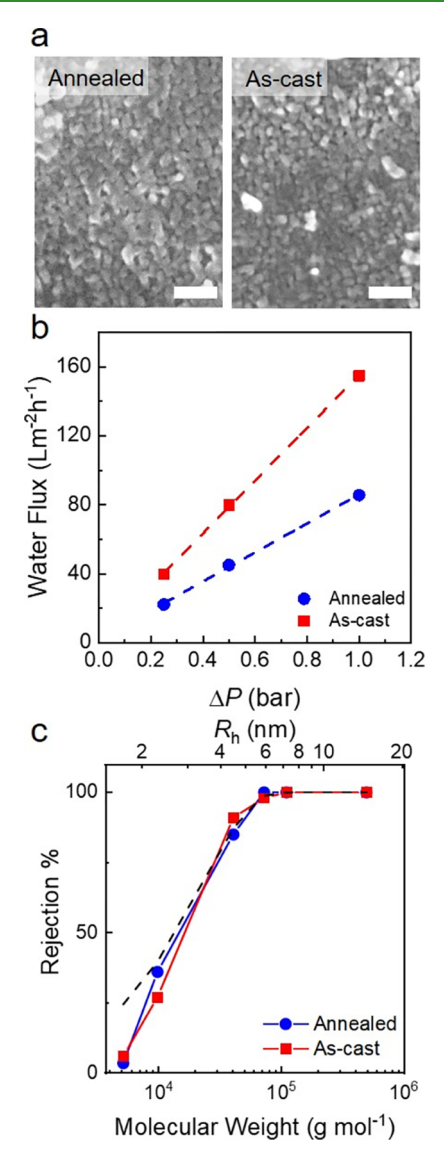


Figure 6. Top-view SEM images (a), water flux as a function of applied pressure difference (b), and true rejection of fluorescently labeled dextran standards (c) for thermally annealed and solvent-disordered as-cast dual-layer membranes fabricated on PSF supports cast from an 18 wt % solution in DMF. The experimental rejection data was corrected using the mass transfer coefficient to account for concentration polarization. The water flux and rejection data are for a representative data set. The scale bar corresponds to 200 nm.

water permeability for the annealed bare PSF support (18 wt % in DMF), 146 \pm 17 L m $^{-2}$ h $^{-1}$ bar $^{-1}$, as compared to the analogous as-cast bare PSF support, 326 \pm 12 L m $^{-2}$ h $^{-1}$ bar $^{-1}$. This decrease in the permeability of the PSF support upon thermal annealing resulted in a subsequent decrease in the permeability of the dual-layer membrane, again suggesting that the PSF support layer primarily dictates the permeability of these dual-layer membranes. 3,40

Contributions of Support and Selective Layers to Dual-Layer Membrane Permeability. To better decouple the relative contributions of the support and selective layers to the dual-layer membrane permeability, the dual-layer membranes were modeled as resistors in series. This model assumes that the resistance to water flow for each layer is inversely proportional to the water permeability (P) of each

layer. Consequently, the water permeability of the dual-layer membrane follows the relationship

$$P_{\text{dual}}^{-1} = P_{\text{support}}^{-1} + P_{\text{selective}}^{-1} \tag{2}$$

While the intrinsic permeability of the selective layer, $P_{\rm selective}$ is difficult to measure directly, it can be readily extracted using eq 2, provided that $P_{\rm dual}$ and $P_{\rm support}$ are experimentally known, as is the case for this work. Using this approach, the effect that thermal annealing had on the water permeability for both the support and selective layers was examined independently.

The experimentally measured values for $P_{\rm dual}$ and $P_{\rm support}$ along with the values of $P_{\rm selective}$ calculated using the model described in eq 2 are provided in Figure 7 and Table S1 for

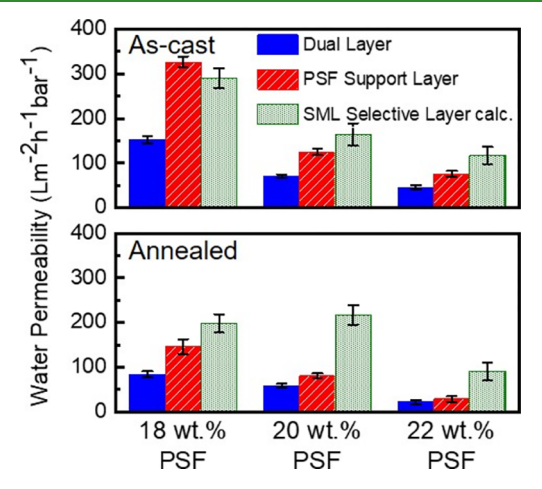


Figure 7. Bar graphs comparing the relative contributions of the PSF support layer (red bars) and the SML-48 selective layer (green bars) to the overall dual-layer membrane permeability (blue bars) for different PSF concentrations. Data for thermally annealed membranes is presented in the lower panel, and data for the as-cast membranes is presented in the upper panel. The dual-layer and PSF support-layer permeabilities were measured experimentally. The selective-layer permeability was calculated using the resistors in the series model described in eq 2. The permeability was determined based on the mean of three separate experiments, and the error bars correspond to the standard deviation.

both annealed and as-cast membranes. As discussed previously, both the concentration of the PSF casting solution and the thermal processing method had a strong effect on the water permeability of the dual-layer membranes (shown as an average of three separate experiments), ranging from 22 \pm 5 L m⁻² h⁻¹ bar⁻¹ for the annealed membrane prepared using a 22 wt % PSF solution to $153 \pm 8 \text{ L m}^{-2} \text{ h}^{-1} \text{ bar}^{-1}$ for the as-cast membrane prepared using an 18 wt % PSF solution. The calculated $P_{\text{selective}}$ ranged from 91 to 290 L m⁻² h⁻¹ bar⁻¹ for all conditions examined here, exhibiting a weaker dependence on the selected processing parameters than P_{support} (i.e., a factor of 3 difference as compared to a factor of 7 difference for the dual-layer membranes). The observed variation in $P_{\text{selective}}$ may reflect slight differences in the segregation strengths between different processing conditions or the existence of concentration effects on the interfacial structure between the layers. The calculated selective layer permeabilities were approxm⁻² h^{-1} bar⁻¹ estimated using the Hagen-Poiseuille equation⁴³

$$P = \frac{\varepsilon r_{\rm p}^{\ 2}}{8\tau^2 \mu \delta_{\rm m}} \tag{3}$$

assuming a porosity (ε) of 0.4 (volume fraction of PLA in SML-48), a tortuosity (τ) of 1.5, a pore radius (r_n) of 6.8 nm, and a film thickness (1) of 200 nm based on the cross-sectional SEM images. The lower experimental permeabilities may reflect that the block polymer selective layer contains some amount of discontinuous pores (e.g., at the selective-layer/ support-layer interface) or a higher than expected pore tortuosity. Overall, the water permeabilities of the dual-layer membranes fabricated by co-casting are higher than the highest water permeabilities that have been previously reported for disordered block polymer selective layers cast onto porous support layers, ca. 10 L m⁻² h⁻¹ bar⁻¹. 22-24 The highest water permeabilities obtained for the dual-layer membranes, 150 L m⁻² h⁻¹ bar⁻¹, are comparable to the highest water permeabilities reported for membranes with selectively etched ordered block polymer selective layers, membranes with selectively swollen block polymer selective layers, and SNIPS membranes with comparable pore size (ca. 15-20 nm), which generally range from 150 to 200 L m⁻² h⁻¹ bar⁻¹.5,16,44,45</sup>

Significant increases in the water permeability for dual-layer membranes composed of an SML-48 selective layer will require engineering approaches to enhance the permeability of the PSF support. However, significantly higher permeabilities (i.e., greater than approximately 220 L m⁻² h⁻¹ bar⁻¹) will also require increasing the porosity and permeability of the SML selective layer. To demonstrate this point, an as-cast dual-layer membrane was fabricated from a 0.05 wt % solution of SML-48 in THF and a 15 wt % solution of PSF in DMF. This membrane displayed very high water permeability of ~250 L m⁻² h⁻¹ bar⁻¹ because of its thinner selective layer and more porous support layer (Figure S15). Additionally, a nearly identical rejection profile to the membranes cast from 0.1 wt % solutions of SML-48 was obtained. However, these low PSF concentrations often resulted in the formation of defective membranes that lacked the required mechanical integrity for UF. For this reason, repeatable fabrication of these membranes was challenging. Consequently, other strategies are likely required to more reproducibly enhance the permeability of the dual-layer membranes. Regardless, the results presented here offer a proof-of-concept for a promising membrane fabrication technique.

CONCLUSIONS

In this work, we have reported a promising technique to prepare highly selective and highly permeable UF membranes with a disordered block polymer selective layer by co-casting PSF and block polymer solutions. A dilute P(MMA-s-S)-b-PLA solution in THF was spin coated onto a DMF-swollen PSF film, rapidly heated or dried at room temperature to disorder the block polymer, and immersed in an ice water coagulation bath to kinetically trap the fluctuating disordered state in the block polymer layer and to precipitate the PSF support layer via NIPS. The subsequent removal of the PLA domains generated a dual-layer UF membrane, as confirmed by SEM. We demonstrated that the permeability of the dual-layer membranes could be tuned by adjusting the concentration of the PSF casting solution while maintaining a nearly identical size-selectivity because of the narrow pore size distribution of the block polymer selective layer. Additionally, we investigated

the effect of thermal processing on the permeability and selectivity of these membranes. Similar morphologies and size-selectivities, yet noticeably higher water permeabilities, could be obtained for solvent-disordered "as-cast" membranes as compared to thermally annealed membranes. Modeling the dual-layer membranes as resistors in series revealed that the porosity of the PSF support layer was the primary influence on the water permeability of the dual-layer membranes.

The membrane fabrication procedure outlined in this work offers a promising approach toward simultaneously achieving high water permeability and high size-selectivity in UF membranes. The overall approach is expected to be compatible with several polymer chemistries and solvents, allowing the membrane properties to be tuned for a targeted application. The approach should also be compatible with draw coating, curtain coating, and hollow fiber membrane fabrication protocols, potentially enabling its translation to more industrially scalable coating processes and relevant form factors. Further optimization of the PSF layer casting parameters should increase the permeability without compromising the size-selectivity and potentially offer a more commercially viable route toward block polymer UF membranes.

ASSOCIATED CONTENT

Supporting Information

The Supporting Information is available free of charge at https://pubs.acs.org/doi/10.1021/acsami.0c13726.

Description of the synthesis of the P(MMA-s-S)-b-PLA block polymer; NMR, SEC, DMA, and SAXS of the block polymer; N₂ sorption of porous monoliths; detailed description of the membrane fabrication process; and water flux, dextran rejection curves, and SEM images of dual-layer and bare PSF membranes (PDF)

AUTHOR INFORMATION

Corresponding Author

Marc A. Hillmyer — Department of Chemistry, University of Minnesota, Minneapolis, Minnesota 55455, United States; orcid.org/0000-0001-8255-3853; Email: hillmyer@umn.edu

Authors

Nicholas Hampu — Department of Chemical Engineering and Materials Science, University of Minnesota, Minneapolis, Minnesota 55455, United States; orcid.org/0000-0002-8127-1034

Jay R. Werber – Department of Chemistry, University of Minnesota, Minneapolis, Minnesota 55455, United States

Complete contact information is available at: https://pubs.acs.org/10.1021/acsami.0c13726

Notes

The authors declare no competing financial interest.

ACKNOWLEDGMENTS

The authors would like to thank Dr. Daphne Chan for helpful advice and Prof. Lorraine Francis for carefully reviewing the manuscript. ALTASORB generously donated lactide. Funding for this work was provided by the National Science Foundation (DMR-1609459 and DMR-2003454). The Hitachi SU8320

microscope was provided by NSF MRI DMR1229263. Parts of this work were carried out in the Characterization Facility, UMN, which receives partial support from NSF through the MRSEC program. Portions of this work were performed at the DuPont-Northwestern-Dow Collaborative Access Team (DND-CAT) located at Sector 5 of the Advanced Photon Source (APS). DND-CAT is supported by the Northwestern University, E.I. DuPont de Nemours & Co., and The Dow Chemical Company. This research used resources of the APS, a U.S. Department of Energy (DOE) Office of Science User Facility operated for the DOE Office of Science by Argonne National Laboratory under contract no. DE-AC02-06CH11357. Data were collected using an instrument funded by the NSF under award number 0960140.

REFERENCES

- (1) Werber, J. R.; Osuji, C. O.; Elimelech, M. Materials for next-Generation Desalination and Water Purification Membranes. *Nat. Rev. Mater.* **2016**, *1*, 16018.
- (2) Park, H. B.; Kamcev, J.; Robeson, L. M.; Elimelech, M.; Freeman, B. D. Maximizing the Right Stuff: The Trade-off between Membrane Permeability and Selectivity. *Science* **2017**, 356, No. eaab0530.
- (3) Guillen, G. R.; Pan, Y.; Li, M.; Hoek, E. M. V. Preparation and Characterization of Membranes Formed by Nonsolvent Induced Phase Separation: A Review. *Ind. Eng. Chem. Res.* **2011**, *50*, 3798–3817.
- (4) Sadeghi, I.; Kaner, P.; Asatekin, A. Controlling and Expanding the Selectivity of Filtration Membranes. *Chem. Mater.* **2018**, *30*, 7328–7354.
- (5) Yang, S. Y.; Park, J.; Yoon, J.; Ree, M.; Jang, S. K.; Kim, J. K. Virus Filtration Membranes Prepared from Nanoporous Block Copolymers with Good Dimensional Stability under High Pressures and Excellent Solvent Resistance. *Adv. Funct. Mater.* **2008**, *18*, 1371–1377.
- (6) Yang, H.; Wang, Z.; Lan, Q.; Wang, Y. Antifouling Ultrafiltration Membranes by Selective Swelling of Polystyrene/poly(ethylene Oxide) Block Copolymers. *J. Membr. Sci.* **2017**, 542, 226–232.
- (7) Mehta, A.; Zydney, A. L. Permeability and Selectivity Analysis for Ultrafiltration Membranes. *J. Membr. Sci.* **2005**, 249, 245–249.
- (8) Smolders, C. A.; Reuvers, A. J.; Boom, R. M.; Wienk, I. M. Microstructures in Phase-Inversion Membranes. Part 1. Formation of Macrovoids. *J. Membr. Sci.* **1992**, *73*, 259–275.
- (9) Mochizuki, S.; Zydney, A. L. Theoretical Analysis of Pore Size Distribution Effects on Membrane Transport. *J. Membr. Sci.* **1993**, 82, 211–227.
- (10) Phillip, W. A.; O'Neill, B.; Rodwogin, M.; Hillmyer, M. A.; Cussler, E. L. Self-Assembled Block Copolymer Thin Films as Water Filtration Membranes. *ACS Appl. Mater. Interfaces* **2010**, *2*, 847–853.
- (11) Yin, J.; Yao, X.; Liou, J.-Y.; Sun, W.; Sun, Y.-S.; Wang, Y. Membranes with Highly Ordered Straight Nanopores by Selective Swelling of Fast Perpendicularly Aligned Block Copolymers. *ACS Nano* **2013**, *7*, 9961–9974.
- (12) Peinemann, K.-V.; Abetz, V.; Simon, P. F. W. Asymmetric Superstructure Formed in a Block Copolymer via Phase Separation. *Nat. Mater.* **2007**, *6*, 992–996.
- (13) Jackson, E. A.; Lee, Y.; Hillmyer, M. A. ABAC Tetrablock Terpolymers for Tough Nanoporous Filtration Membranes. *Macro-molecules* **2013**, *46*, 1484–1491.
- (14) Querelle, S. E.; Jackson, E. A.; Cussler, E. L.; Hillmyer, M. A. Ultrafiltration Membranes with a Thin Poly(styrene)-B-Poly(isoprene) Selective Layer. ACS Appl. Mater. Interfaces 2013, 5, 5044–5050.
- (15) Feng, X.; Tousley, M. E.; Cowan, M. G.; Wiesenauer, B. R.; Nejati, S.; Choo, Y.; Noble, R. D.; Elimelech, M.; Gin, D. L.; Osuji, C. O. Scalable Fabrication of Polymer Membranes with Vertically

- Aligned 1 Nm Pores by Magnetic Field Directed Self-Assembly. ACS Nano 2014, 8, 11977—11986.
- (16) Phillip, W. A.; Dorin, R. M.; Werner, J.; Hoek, E. M. V.; Wiesner, U.; Elimelech, M. Tuning Structure and Properties of Graded Triblock Terpolymer-Based Mesoporous and Hybrid Films. *Nano Lett.* **2011**, *11*, 2892–2900.
- (17) Shi, X.; Wang, Z.; Wang, Y. Highly Permeable Nanoporous Block Copolymer Membranes by Machine-Casting on Nonwoven Supports: An Upscalable Route. *J. Membr. Sci.* **2017**, 533, 201–209.
- (18) Yan, N.; Wang, Z.; Wang, Y. Highly Permeable Membranes Enabled by Film Formation of Block Copolymers on Water Surface. *J. Membr. Sci.* **2018**, *568*, 40–46.
- (19) Wang, Y. Nondestructive Creation of Ordered Nanopores by Selective Swelling of Block Copolymers: Toward Homoporous Membranes. *Acc. Chem. Res.* **2016**, *49*, 1401–1408.
- (20) Dorin, R. M.; Marques, D. S.; Sai, H.; Vainio, U.; Phillip, W. A.; Peinemann, K.-V.; Nunes, S. P.; Wiesner, U. Solution Small-Angle X-Ray Scattering as a Screening and Predictive Tool in the Fabrication of Asymmetric Block Copolymer Membranes. *ACS Macro Lett.* **2012**, *1*, 614–617.
- (21) Abetz, V. Isoporous Block Copolymer Membranes. *Macromol. Rapid Commun.* **2015**, 36, 10–22.
- (22) Vidil, T.; Hampu, N.; Hillmyer, M. A. Nanoporous Thermosets with Percolating Pores from Block Polymers Chemically Fixed above the Order–Disorder Transition. *ACS Cent. Sci.* **2017**, *3*, 1114–1120.
- (23) Hampu, N.; Hillmyer, M. A. Temporally Controlled Curing of Block Polymers in the Disordered State Using Thermally Stable Photoacid Generators for the Preparation of Nanoporous Membranes. ACS Appl. Polym. Mater. 2019, 1, 1148–1154.
- (24) Hampu, N.; Bates, M. W.; Vidil, T.; Hillmyer, M. A. Bicontinuous Porous Nanomaterials from Block Polymers Radically Cured in the Disordered State for Size-Selective Membrane Applications. ACS Appl. Nano Mater. 2019, 2, 4567–4577.
- (25) Hampu, N.; Hillmyer, M. A. Molecular Engineering of Nanostructures in Disordered Block Polymers. *ACS Macro Lett.* **2020**, *9*, 382–388.
- (26) Hilke, R.; Pradeep, N.; Behzad, A. R.; Nunes, S. P.; Peinemann, K.-V. Block Copolymer/homopolymer Dual-Layer Hollow Fiber Membranes. *J. Membr. Sci.* **2014**, 472, 39–44.
- (27) Liu, Y.; Liu, T.; Su, Y.; Yuan, H.; Hayakawa, T.; Wang, X. Fabrication of a Novel PS4VP/PVDF Dual-Layer Hollow Fiber Ultrafiltration Membrane. *J. Membr. Sci.* **2016**, *506*, 1–10.
- (28) Seo, M.; Hillmyer, M. A. Reticulated Nanoporous Polymers by Controlled Polymerization-Induced Microphase Separation. *Science* **2012**, 336, 1422.
- (29) Gor, G. Y.; Thommes, M.; Cychosz, K. A.; Neimark, A. V. Quenched Solid Density Functional Theory Method for Characterization of Mesoporous Carbons by Nitrogen Adsorption. *Carbon* **2012**, *50*, 1583–1590.
- (30) Tiraferri, A.; Yip, N. Y.; Phillip, W. A.; Schiffman, J. D.; Elimelech, M. Relating Performance of Thin-Film Composite Forward Osmosis Membranes to Support Layer Formation and Structure. J. Membr. Sci. 2011, 367, 340–352.
- (31) Oatley-Radcliffe, D. L.; Williams, S.; Lee, C.; Williams, P. Characterisation of Mass Transfer in Frontal Nanofiltration Equipment and Development of a Simple Correlation. *J. Membr. Sep. Technol.* **2015**, *4*, 149–160.
- (32) Zhang, Y.; Sargent, J. L.; Boudouris, B. W.; Phillip, W. A. Nanoporous Membranes Generated from Self-Assembled Block Polymer Precursors: Quo Vadis? *J. Appl. Polym. Sci.* 2015, 132, 41683.
- (33) Phillip, W. A.; Amendt, M.; O'Neill, B.; Chen, L.; Hillmyer, M. A.; Cussler, E. L. Diffusion and Flow Across Nanoporous Polydicyclopentadiene-Based Membranes. *ACS Appl. Mater. Interfaces* **2009**, *1*, 472–480.
- (34) Lodge, T. P.; Hanley, K. J.; Pudil, B.; Alahapperuma, V. Phase Behavior of Block Copolymers in a Neutral Solvent. *Macromolecules* **2003**, *36*, 816–822.
- (35) Baruth, A.; Seo, M.; Lin, C. H.; Walster, K.; Shankar, A.; Hillmyer, M. A.; Leighton, C. Optimization of Long-Range Order in

- Solvent Vapor Annealed Poly(styrene)-Block-Poly(lactide) Thin Films for Nanolithography. ACS Appl. Mater. Interfaces 2014, 6, 13770–13781.
- (36) Sinturel, C.; Vayer, M.; Morris, M.; Hillmyer, M. A. Solvent Vapor Annealing of Block Polymer Thin Films. *Macromolecules* **2013**, 46, 5399–5415.
- (37) Hur, S.-M.; Khaira, G. S.; Ramírez-Hernández, A.; Müller, M.; Nealey, P. F.; de Pablo, J. J. Simulation of Defect Reduction in Block Copolymer Thin Films by Solvent Annealing. *ACS Macro Lett.* **2015**, *4*, 11–15.
- (38) Howard, M. P.; Lequieu, J.; Delaney, K. T.; Ganesan, V.; Fredrickson, G. H.; Truskett, T. M. Connecting Solute Diffusion to Morphology in Triblock Copolymer Membranes. *Macromolecules* **2020**, *53*, 2336–2343.
- (39) Olayo-Valles, R.; Guo, S.; Lund, M. S.; Leighton, C.; Hillmyer, M. A. Perpendicular Domain Orientation in Thin Films of Polystyrene–Polylactide Diblock Copolymers. *Macromolecules* **2005**, 38, 10101–10108.
- (40) Tsai, H.-A.; Huang, D.-H.; Ruaan, R.-C.; Lai, J.-Y. Mechanical Properties of Asymmetric Polysulfone Membranes Containing Surfactant as Additives. *Ind. Eng. Chem. Res.* **2001**, *40*, 5917–5922.
- (41) Werber, J. R.; Porter, C. J.; Elimelech, M. A Path to Ultraselectivity: Support Layer Properties To Maximize Performance of Biomimetic Desalination Membranes. *Environ. Sci. Technol.* **2018**, 52, 10737–10747.
- (42) Henis, J. M. S.; Tripodi, M. K. Composite Hollow Fiber Membranes for Gas Separation: The Resistance Model Approach. *J. Membr. Sci.* **1981**, *8*, 233–246.
- (43) Epstein, N. On tortuosity and the tortuosity factor in flow and diffusion through porous media. *Chem. Eng. Sci.* **1989**, 44, 777–779.
- (44) Ahn, H.; Park, S.; Kim, S.-W.; Yoo, P. J.; Ryu, D. Y.; Russell, T. P. Nanoporous Block Copolymer Membranes for Ultrafiltration: A Simple Approach to Size Tunability. *ACS Nano* **2014**, *8*, 11745–11752.
- (45) Dorin, R. M.; Phillip, W. A.; Sai, H.; Werner, J.; Elimelech, M.; Wiesner, U. Designing Block Copolymer Architectures for Targeted Membrane Performance. *Polymer* **2014**, *55*, 347–353.